Organic Electronics 15 (2014) 2624–2631

Contents lists available at ScienceDirect

Organic Electronics

journal homepage: www.elsevier.com/locate/orgel

Comparison of dimethyl sulfoxide treated highly conductive poly(3,4-ethylenedioxythiophene):poly(styrenesulfonate) electrodes for use in indium tin oxide-free organic electronic photovoltaic devices

N.K. Unsworth [a], I. Hancox [a], C. Argent Dearden [a], P. Sullivan [a], M. Walker [b], R.S. Lilley [c], J. Sharp [c], T.S. Jones [a,*]

[a] Department of Chemistry, University of Warwick, Coventry CV4 7AL, UK
[b] Department of Physics, University of Warwick, Coventry CV4 7AL, UK
[c] Paintbox Limited, 36-44 Melchett Road, Birmingham B30 3HS, UK

ARTICLE INFO

Article history:
Received 16 April 2014
Received in revised form 23 June 2014
Accepted 11 July 2014
Available online 24 July 2014

Keywords:
Organic photovoltaic devices
Poly(3,4-ethylenedioxythiophene)
poly(styrenesulfonate)
Indium tin oxide-free
Conductive atomic force microscopy

ABSTRACT

Indium tin oxide (ITO)-free organic photovoltaic (OPV) devices were fabricated using highly conductive poly(3,4-ethylenedioxythiophene):poly(styrenesulfonate) (PEDOT:PSS) as the transparent conductive electrode (TCE). The intrinsic conductivity of the PEDOT:PSS films was improved by two different dimethyl sulfoxide (DMSO) treatments – (i) DMSO was added directly to the PEDOT:PSS solution (PEDOT:PSS_{ADD}) and (ii) a pre-formed PEDOT:PSS film was immersed in DMSO (PEDOT:PSS_{IMM}). X-ray photoelectron spectroscopy (XPS) and conductive atomic force microscopy (CAFM) studies showed a large amount of PSS was removed from the PEDOT:PSS_{IMM} electrode surface. OPV devices based on a poly(3-hexylthiophene):[6,6]-phenyl-C_{61}-butyric acid methyl ester (P3HT:PCBM) bulk hetrojunction showed that the PEDOT:PSS_{IMM} electrode out-performed the PEDOT:PSS_{ADD} electrode, primarily due to an increase in short circuit current density from 6.62 mA cm^{-2} to 7.15 mA cm^{-2}. The results highlight the importance of optimising the treatment of PEDOT:PSS electrodes and demonstrate their potential as an alternative TCE for rapid processing and low-cost OPV and other organic electronic devices.

1. Introduction

Organic photovoltaic (OPV) devices are attracting increasing interest as a cheap alternative renewable energy source. The OPV device architecture typically comprises of a photoactive layer and blocking or transporting layers sandwiched between two electrodes, with the total device being only a few hundred nanometres thick. Recent advancements, such as new photoactive materials, material stability, and processing onto flexible substrates have highlighted their potential for mass production [1–3]. The main advantages of OPV devices over their inorganic counterparts are thought to be the high manufacturing speeds and low temperature processing involved. To help maximise these benefits an alternative transparent conductive electrode (TCE) to the widely used indium–tin oxide (ITO) needs to be found. ITO is generally used as the TCE due to its low sheet resistance (R_{sheet}) and high optical transparency, however the ITO electrode is fabricated by a vacuum sputtering process which is expensive and energy intensive. Additionally, the limited availability and high demand for indium has also contributed to its

* Corresponding author. Tel.: +44 (0)2476528265; fax: +44 (0)2476524112.
E-mail address: t.s.jones@warwick.ac.uk (T.S. Jones).

http://dx.doi.org/10.1016/j.orgel.2014.07.015
1566-1199/

high cost. A study by Azzopardi et al. attributed 38–51% of the total cost of an OPV device to the ITO electrode [4]. This high cost, along with limited energetic compatibility with frequently used photoactive organic materials, poor flexibility and tendency to crack and/or delaminate, has resulted in a strong interest to find an alternative material for use as the TCE without these disadvantages. Several different materials have been investigated including graphene [5], carbon nanotubes [6], thin metal films [7], metal grids [8], nanowires [9], and conducting polymers [10].

Poly(3,4-ethylenedioxythiophene):poly(styrenesulfonate) (PEDOT:PSS), an intrinsically conducting polymer, has been extensively studied. PEDOT:PSS first found use as an antistatic layer in photographic film [11], followed by widespread use as a transparent conductive layer in electroluminescent devices, capacitors, and transistors, and as a hole injection layer in organic light emitting diodes (OLEDs) [10]. In OPV devices, PEDOT:PSS has been extensively used as a hole transport layer as it produces a higher work function than ITO resulting in a better energetic alignment with many commonly used organic electron donor materials [12,13]. PEDOT:PSS also helps to planarize the inhomogeneous ITO surface thereby improving the interface with the photoactive material [13]. The high transparency, low cost, flexible applications, and compatibility with spray and printing technologies has seen PEDOT:PSS emerge as a particularly promising alternative to ITO despite concerns over its acidity and hygroscopicity [14,15].

Despite being considered conductive, the conductivity of PEDOT:PSS films are much lower than that of ITO. Many different methods to improve the conductivity have been reported; these include the addition of a small volume percentage (vol-%) of surfactants [16], ionic liquids [17], polyols [18], and polar organic solvents to the PEDOT:PSS dispersion [19]. The conductivity can also be enhanced by post-treatment of the PEDOT:PSS film. sulphuric acid [20], and low boiling point organic solvents such as methanol and ethanol used singularly or as a co-solvent can be dropped onto a PEDOT:PSS film [21,22]. Immersing pre-formed PEDOT:PSS films in a polar organic solvent like ethylene glycol has also been shown to improve the intrinsic conductivity of PEDOT:PSS films [23]. Despite extensive efforts into improving the conductivity, understanding how each respective method affects the PEDOT:PSS conductivity continues to be widely discussed in literature.

Within this wide range of methods, the use of polar organic solvents such as dimethyl sulfoxide (DMSO) and ethylene glycol have been shown to reliably increase the conductivity of PEDOT:PSS thin films. Despite the substantial amount of literature related to explaining the improvement in conductivity the mechanism is still widely debated. Screening effects between PEDOT and PSS chains due to the polar solvent [19], enhanced charge mobility due to an improved interchain packing and thinner PSS barriers [24,25], and a more uniform distribution of PEDOT-rich regions are just some of the proposed mechanisms [26]. Post-treatment of a PEDOT:PSS film by immersion in a polar organic solvent has been shown to turn the film insoluble and improve the conductivity by removing PSS [23,27,28].

While the use of polar organic solvents with PEDOT:PSS, either by addition to the initial dispersion or via a post-film treatment, have been shown to result in conductive films that are suitable for use in OPV devices, few studies have directly compared the two preparation methods. Here we present a direct comparison of two different preparation methods of PEDOT:PSS TCEs treated with DMSO. The DMSO was either added to the PEDOT:PSS solution (PEDOT:PSS_{ADD}) or the pre-formed PEDOT:PSS film was immersed in DMSO for a predetermined time (PEDOT:PSS_{IMM}). We demonstrate conductive atomic force microscopy (CAFM) as a powerful tool for investigating the distribution of PEDOT and PSS on the electrode surface, and this is combined with X-ray photoelectron spectroscopy (XPS), ultraviolet–visible spectroscopy (UV–Vis), kelvin probe and contact angle measurements to allow further insight into the effect DMSO has on the PEDOT:PSS electrode. A well characterised photoactive system, the poly(3-hexylthiophene):[6,6]-phenyl-C_{61}-butyric acid methyl ester (P3HT:PCBM) bulk hetrojunction, was then used to study the effect both treatments have on the resulting OPV device performance. OPV devices using PEDOT:PSS_{IMM} electrodes slightly out performed those using PEDOT:PSS_{ADD} electrodes. This promising device performance for DMSO treated PEDOT:PSS electrodes combined with their lower cost indicate the possibility of using PEDOT:PSS as an alternative TCE in low cost roll-to-roll processed OPV devices.

2. Experimental details

2.1. Preparation and characterisation of the PEDOT:PSS electrodes

PEDOT:PSS (Clevios PH1000) dispersions purchased from Heraeus Holding GmbH were prepared prior to spin-coating onto glass substrates (12 × 12 mm) that were cleaned by a four-step solvent cleaning process, followed by an ultraviolet/ozone treatment to remove any carbon residues. The PEDOT:PSS_{ADD} solution was prepared by adding DMSO (5 vol-%) to the as-bought PEDOT:PSS dispersion. Untreated PEDOT:PSS (PEDOT:PSS_{UT}) and PEDOT: PSS_{IMM} electrodes were formed using as-bought PEDOT:PSS. Each solution was filtered (0.45 μm, PVDF) at room temperature onto the glass substrate and spin-coated at 2000 RPM for 60 s. The electrodes were then annealed on a hot plate at 110 °C for 20 min in an ambient atmosphere. The PEDOT:PSS_{IMM} films were then cooled to room temperature, and then immersed in DMSO for 30 min before being placed on a hot plate at 110 °C until dry. All films were allowed to cool to room temperature before further measurements were carried out.

The R_{sheet} of the electrodes was measured using the four-point probe Van der Pauw method with a Keithley 2400 sourcemeter current source and Fluke 179 True RMS multimeter. UV–Vis electronic absorption spectra were obtained using a Perkin–Elmer 25 spectrometer. PEDOT:PSS films were spin coated at 2000 RPM onto pre-cleaned quartz substrates for UV–Vis measurements. XPS measurements were taken using a monochromated X-ray Al Kα source (Omicron XM 1000, $h\upsilon$ = 1486.6 eV) and the photoelectrons were detected with an Omicron Sphera electron analyser in

an ultra-high vacuum system with a base pressure of $\sim 2 \times 10^{-11}$ mbar. All XPS spectra were referenced to the C–(C, H) peak observed in the C 1s region at 284.6 eV, and fitted in CasaXPS using a Shirley background and mixed Gaussian–Lorentzian lineshapes for oxygen and sulphur. Asymmetric lineshapes were required for the PEDOT components in the S 2p region [29], achieved via the use of Gaussian–Lorentzian lineshapes modified by an exponential blend on the high binding energy tail. AFM images were obtained using an Asylum Research MFP-3D (Santa Barbara, USA) in AC mode. The MFP-3D was fitted with an ORCA integrated tip-holder and current preamplifier (20 nA) for CAFM measurements. Both the topography and current distribution images were obtained simultaneously using Au/Cr coated cantilevers (Olympus TR400 PB, tip radius < 40 nm, spring constant 0.02 N m^{-1}). Surface work function measurements were obtained using a kelvin probe under a nitrogen atmosphere and referenced to freshly cleaved highly ordered pyrolytic graphite. A Krüss drop shape analyser system DSA100 with tilting table was used to carry out contact angle measurements under an ambient atmosphere.

2.2. Fabrication and characterisation of OPV devices

OPV devices were fabricated using the three PEDOT:PSS electrodes and the ITO (Thin Film Devices, 145 nm thick, R_{sheet} < 15 Ω sq^{-1}) electrodes. A less conductive PEDOT:PSS dispersion (Clevios P VP 4083, Heraeus, PEDOT:PSS_{HTL}) was filtered (0.45 μm, PVDF) and spin-coated (3000 RPM, 60 s) on top of the ITO electrode and annealed as above. The P3HT:PCBM photoactive layer was prepared by stirring 20 mg mL^{-1} of P3HT (regioregular, Reike Metals) and PCBM (99.5%, Solenne BV) in 1,2-dichlorobenzene at 40 °C for 24 h. The P3HT:PCBM solution was then filtered (0.2 μm, PTFE) and spin-coated at 800 RPM for 60 s onto the respective electrodes. The spin-coated films were covered with a petri dish lid to dry slowly, and once dried the films were annealed at 120 °C for 20 min to form an active layer thickness of ~130 nm. All P3HT:PCBM processing steps were performed in a nitrogen environment. The substrates were then transferred into a Kurt J. Lesker Spectros system where bathocuproine (BCP, Aldrich, 8 nm) was vapour deposited on top of the P3HT:PCBM films. The aluminium (Al) top contact was deposited through an electrode shadow mask to give an active area of 0.06 cm^2.

Current–density (*J–V*) measurements were recorded using a Keithley 2400 sourcemeter with simulated AM1.5G solar illumination at 100 ± 2 mW cm^{-2} (1.00 ± 0.02 sun), calibrated for each device using a Fraunhofer calibrated silicon photodiode (PV Measurements Inc.). External quantum efficiency measurements (EQE) were carried out using a Sciencetech SF150 xenon arc lamp and a PTI Monochromator, calibrated with a Si photodiode (Newport 818-UV). The signal was detected with a current–voltage amplifier (Femto DHPCA-100) and lock-in amplifier (Stanford Research SR 830 DSP).

3. Results and discussion

The R_{sheet} value for the PEDOT:PSS_{UT} electrode was high at over 200,000 Ω sq^{-1}. Using DMSO, by both addition and immersion, the R_{sheet} was decreased to 208 Ω sq^{-1} (standard deviation (σ) = 24 Ω sq^{-1}) and 214 Ω sq^{-1} (σ = 39 Ω sq^{-1}) for PEDOT:PSS_{ADD} and PEDOT:PSS_{IMM} respectively, which is just one order of magnitude greater than that of ITO (15 Ω sq^{-1}). The PEDOT:PSS_{UT} and PEDOT:PSS_{ADD} electrodes produced films with a similar film thickness of 90 nm and 86 nm respectively. However, a 36% decrease in film thickness was observed for PEDOT:PSS_{IMM} (58 nm) electrodes, consistent with previous findings [23,28,30]. Neither DMSO treatment resulted in a significant change in transmittance across the visible region, indicating very little PEDOT was removed, as seen in Fig. 1. The inset of Fig. 1 shows the absorption peak at 225 nm, attributed to absorption from the phenyl rings in the PSS [31]. A similar absorption peak was seen for both PEDOT:PSS_{UT} and PEDOT:PSS_{ADD} electrodes, but a large decrease was observed for the PEDOT:PSS_{IMM} electrodes. This coupled with the film thickness measurements indicates that immersing a PEDOT:PSS film in DMSO removes a large amount of PSS from the film.

XPS was used to investigate the near-surface PSS content in relation to PEDOT for each PEDOT:PSS electrode. The S 2p and O 1s regions for the PEDOT:PSS_{UT} electrodes are shown in Fig. 2a and b respectively. The peaks were deconvolved following previous work by Greczynski et al. [29,32]. The S 2p spectrum shows three main chemical species, two that were assigned to the PSS component (Fig. 2d and e) and one to PEDOT (Fig. 2f), allowing the near surface PEDOT-to-PSS ratio to be determined. The lower binding energy peaks at 164.0 eV and 165.1 eV correspond to the spin–orbit contributions from the S $2p_{3/2}$ and S $2p_{1/2}$ levels from the PEDOT. Asymmetric tails are seen on the higher binding energy side of the two PEDOT components due to the cationic charge of the $PEDOT:PSS^+$ being delocalised over several adjacent thiophene rings. The broad higher binding energy peak near 168 eV is assigned to the PSS sulphur atoms and can be split into PSSH and PSS^-–Na^+ components. The higher energy spin orbit component (yellow line) is assigned to the PSSH components with the S $2p_{3/2}$ peak at 169.0 eV and the S $2p_{1/2}$ peak at 170.2 eV. The lower binding energy component

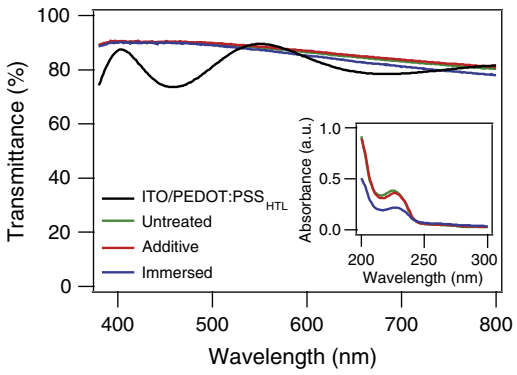

Fig. 1. Transmission spectra of the ITO/PEDOT:PSS_{HTL}, PEDOT:PSS_{UT}, PEDOT:PSS_{ADD} and PEDOT:PSS_{IMM} electrodes. Inset: absorbance of PEDOT:PSS_{UT}, PEDOT:PSS_{ADD} and PEDOT:PSS_{IMM} electrodes between 200 nm and 300 nm.

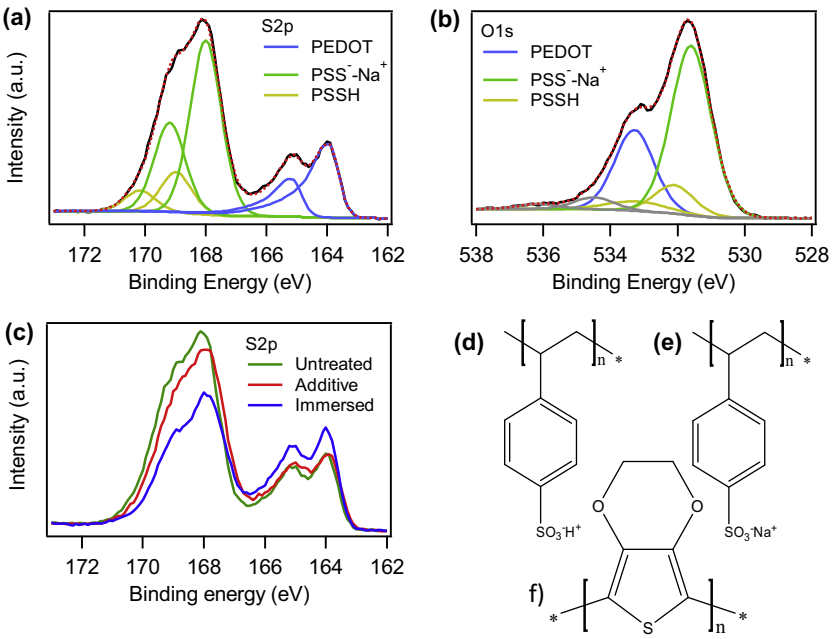

Fig. 2. XPS spectra of (a) the S 2p and (b) the O 1s region for the PEDOT:PSS_{UT} electrode and (c) the S 2p region for the PEDOT:PSS_{UT}, PEDOT:PSS_{ADD} and PEDOT:PSS_{IMM} electrodes. Also shown are the structures of the three main chemical species; (d) PSS^{-}–Na^{+}, (e) PSSH and (f) PEDOT.

corresponds to the PSS^{-}–Na^{+} (green line) with the S $2p_{3/2}$ peak at 168.0 eV and the S $2p_{1/2}$ peak at 169.2 eV. The O 1s spectra (Fig. 2b) again allows the PEDOT and PSS components to be resolved. The peak at 533.3 eV is due to the oxygen atoms in the dioxyethylene bridge in PEDOT. Two PSSH components can be seen (yellow line), the major peak at 532.1 eV corresponds to the oxygen atoms in the sulfonic groups and the broader minor peak at 533.4 eV originates from the hydroxyl oxygen atoms. The intensity ratio of 2:1 agrees with the chemical composition of PSSH. The peak due to the PSS^{-}–Na^{+} component can be seen at 531.6 eV. The other peaks at higher binding energies are assigned to carbon monoxide and residual water contaminants.

The PEDOT-to-PSS ratio obtained from the S 2p and O 1s spectra for the PEDOT:PSS_{UT} electrodes were in good agreement at 1:2.4 and 1:2.6 respectively. The peak deconvolutions were kept constant for both the PEDOT:PSS_{ADD} and PEDOT:PSS_{IMM} electrodes, giving ratios of 1:2.2 and 1:1.5 respectively, as can be seen in Fig. 2c and Table 1. This corresponds to decreases of 12% and 40% in the PSS component of the near-surface region for PEDOT:PSS_{ADD} and PEDOT:PSS_{IMM} electrodes respectively. The information depth was estimated to be ~8 nm, given the inelastic mean free path of 27 Å for S 2p electrons through the material, and the 90 degree take-off angle (with respect to the surface plane) employed in this work [33]. This complements the UV–Vis spectra (inset Fig. 1), showing that a post-treatment immersion with DMSO results in a large decrease in the surface PSS content.

Table 1
Relative ratios between chemical species in PEDOT:PSS_{UT}, PEDOT:PSS_{ADD} and PEDOT:PSS_{IMM} electrodes derived from XPS analysis.

Electrode	PEDOT/PSS ratio	
	S 2p	O 1s
PEDOT:PSS_{UT}	1:2.4	1:2.6
PEDOT:PSS_{ADD}	1:2.0	1:2.4
PEDOT:PSS_{IMM}	1:1.2	1:1.7

Since excess PSS is reported to segregate to the top of PEDOT:PSS_{UT} thin films [25,32], CAFM was used to investigate how this segregation effects the homogeneity of the conductivity of the PEDOT:PSS electrode surfaces. Fig. 3 shows simultaneously obtained CAFM topography, current distribution maps and histograms of the PEDOT:PSS_{UT}, PEDOT:PSS_{ADD} and PEDOT:PSS_{IMM} electrodes. PEDOT:PSS_{UT} electrodes have a smoother surface topography with a surface roughness of 0.9 nm compared to PEDOT:PSS_{ADD} and PEDOT:PSS_{IMM}, which both have a slightly larger surface roughness of 1.2 nm. However, a stark difference in the current distribution maps (Fig. 3d–f) is seen between the PEDOT:PSS electrodes, which is further illustrated by the current distribution histograms (Fig. 3g–i) for each image. The PEDOT:PSS_{UT} electrode surface consists predominantly of non-conducting regions with randomly scattered conductive grains 12–26 nm in diameter, as previously reported [34–36]. The conductive regions (see supplementary information S.I. 1c) are assigned to surface regions of PEDOT, with the insulating areas attributed to PSS. The conductive regions appear to be independent from the topography, showing that PEDOT does not follow any topological features, and is randomly distributed during film formation (S.I. 1d). When compared to PEDOT:PSS_{UT} electrodes, the surface of PEDOT:PSS_{ADD} and PEDOT:PSS_{IMM} electrodes are covered by a significantly higher proportion of conductive regions. The difference in conductivity can

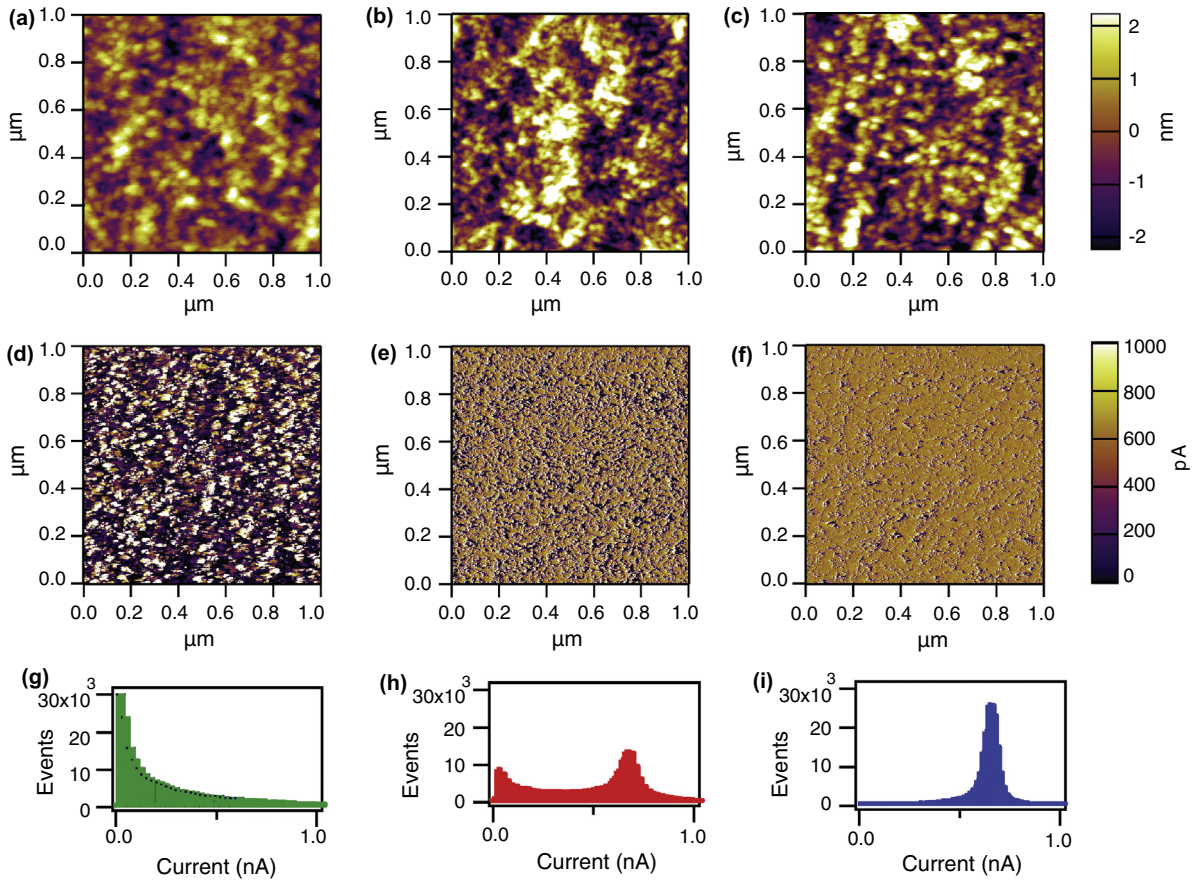

Fig. 3. CAFM topography (a–c), current distribution maps at +320 mV (d–f) and current distribution histograms (g–i) for PEDOT:PSS_{UT} (a, d, g), PEDOT:PSS_{ADD} (b, e, h) and PEDOT:PSS_{IMM} (c, f, i) electrodes.

be more easily seen from the current distribution histograms. Fig. 3d and g show that the vast majority of the PEDOT:PSS_{UT} surface is non-conductive, with a large peak at 0 nA in the current distribution (Fig. 3g), and only a small proportion of the electrode surface showing conductive character. For the PEDOT:PSS_{ADD} electrodes (Fig. 3e and h), the current distribution map and histogram show a distribution of conductivities. The proportion of non-conductive regions is greatly reduced to less than a third of that of PEDOT:PSS_{UT}. A new dominant peak 0.64 nA, can be seen due to the conductive nature of the surface. This peak represents the saturation current of the measurement and does not representative a quantitative value but rather gives a qualitative indication of areas of high conductivity on the film surface. However, a significant part of the electrode surface shows an intermediate conductive behaviour between the peak at 0 nA and the peak at 0.64 nA, which is not as insulating or conductive as other regions. The PEDOT:PSS_{IMM} electrodes display a peak at 0.64 nA in the current distribution histogram (Fig. 3i) of a far greater magnitude, with no discernable peak at 0 nA. The current distribution map (Fig. 3f) also indicates the electrode has the largest coverage of conductive regions. The intermediate behaviour, shown by the PEDOT:PSS_{ADD} electrodes, is not seen for PEDOT:PSS_{IMM} electrodes with the majority of the electrode surface displaying conductive behaviour.

Both DMSO treatments improve the conductivity of the PEDOT:PSS electrodes by a similar magnitude compared to PEDOT:PSS_{UT}, however the CAFM, XPS and UV–Vis studies all show that the enhancement is a result of different modifications to the film. Immersing PEDOT:PSS films in DMSO removes excess PSS from the film, particularly in the near surface region [22,28,38]. The removal of PSS creates a more homogeneous and conductive surface. Adding DMSO to the PEDOT:PSS solution is thought to cause the PEDOT and PSS to rearrange into a more favourable conformation within the film [18]. Studies have suggested that this results in an expanded and more linear PEDOT chain conformation thereby increasing intra and interchain charge carrier mobility or a better three-dimensional network leading to favourable conduction pathways [27,37,38].

The work function of the PEDOT:PSS electrodes was measured using Kelvin probe under a nitrogen environment. The work function decreased from 5.2 eV for both the PEDOT:PSS_{UT} and PEDOT:PSS_{ADD} electrodes to 4.9 eV for the PEDOT:PSS_{IMM} electrodes. This decrease in work function is consistent with the removal of PSS from the PEDOT:PSS film surface due to the removal of the surface

dipole, as shown previously by Nardes et al. [18]. The change in surface composition also resulted in a change in the surface energy between PEDOT:PSS_{ADD} and PEDOT:PSS_{IMM} electrodes, as shown in Fig. 4. The PEDOT:PSS_{ADD} electrodes have a more hydrophilic surface with a contact angle of 27° whereas PEDOT:PSS_{IMM} electrodes, with a lower concentration of PSS on the surface, have a higher contact angle of 59°. The surface energy of the substrate has been shown to affect the segregation of the subsequently spin-coated polymer blends, with a lower surface energy substrate favouring the lower surface energy blend component [39].

The three PEDOT:PSS electrodes were directly compared to an ITO/PEDOT:PSS_{HTL} reference in OPV devices with the following architecture: electrode/P3HT:PCBM/BCP/Al. This extensively studied bulk heterojunction system provides a reliable indication of OPV device performance and the feasibility of using the different PEDOT:PSS electrodes as a replacement for ITO. A less conductive PEDOT:PSS dispersion (PEDOT:PSS_{HTL}) was used as an interfacial layer between the ITO electrode and the P3HT:PCBM photoactive layer [12].

The film thicknesses for the ITO/PEDOT:PSS_{HTL}, PEDOT:PSS_{UT}, PEDOT:PSS_{ADD} and PEDOT:PSS_{IMM} electrodes were first separately optimised by varying the spin speed during spin coating to give optimum device performance (data not shown) before direct comparison. The PEDOT:PSS_{HTL} layer was spin coated at 3000 RPM to give a film thickness of 37 nm on top of the ITO electrode, the PEDOT:PSS_{UT} electrode was spin coated at 2000 RPM to give a film thickness of 90 nm and the PEDOT:PSS_{ADD} and PEDOT:PSS_{IMM} electrodes were spin coated at 3000 RPM and 2000 RPM to give film thicknesses of 68 nm and 58 nm respectively. The annealing process was kept the same for all electrodes; after spin coating with the appropriate PEDOT:PSS dispersion the substrates were annealed at 110 °C for 20 min. The films were then allowed to cool before being immersed in DMSO or being transferred into the glovebox. The transmittance spectra for the optimised electrodes on glass are shown in S.I. 2. Multiple devices were made and tested over a five month period, the averaged current density–voltage (*J–V*) curves are shown in Fig. 5 and the averaged device parameters including the standard deviation are summarised in Table 2. Box and whisker plots displaying device variability are shown in S.I. 3. Devices deposited on ITO/PEDOT:PSS_{HTL} have a short circuit current density (J_{sc}) of 8.46 mA cm^{-2}, an open circuit voltage (V_{oc}) of 0.58 V and a fill factor (*FF*) of 0.60, producing a power conversion efficiency (*PCE*) of 3.00%. Owing to a very high R_{sheet}, PEDOT:PSS_{UT} films acted as poor electrodes, giving poor performing devices, with a PCE of just 0.10%. By contrast, the lower R_{sheet} of the PEDOT:PSS_{ADD} and PEDOT:PSS_{IMM} electrodes allowed for comparable device performance to the ITO reference, with PEDOT:PSS_{ADD} and PEDOT:PSS_{IMM} electrodes resulting in a *PCE* of 2.42% and 2.66% respectively. Both DMSO treated electrodes produced a similar V_{oc} and *FF* with the main difference in device performance due to the higher J_{sc} obtained for the PEDOT:PSS_{IMM} electrodes. PEDOT:PSS_{ADD} had a lower J_{sc} at 6.62 mA cm^{-2} compared to 7.15 mA cm^{-2} for PEDOT:PSS_{IMM}. This improvement in J_{sc} can also be seen from the external quantum efficiency (*EQE*) results shown in S.I. 4.

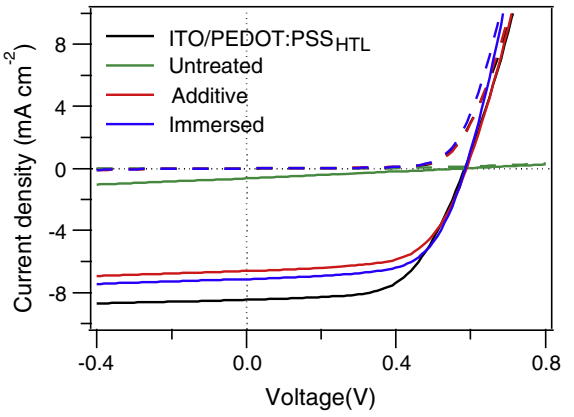

Fig. 5. *J–V* curves under 1 sun illumination (solid lines) and in the dark (dashed lines) for P3HT:PCBM OPV devices with ITO/PEDOT:PSS_{HTL}, PEDOT:PSS_{UT}, PEDOT:PSS_{ADD} and PEDOT:PSS_{IMM} electrodes.

As there is no apparent change in the P3HT:PCBM morphology (S.I. 5), film thickness or absorbance, we propose the following as possible explanations for this 10% increase in J_{sc} for PEDOT:PSS_{IMM} over PEDOT:PSS_{ADD} electrodes. PEDOT:PSS_{IMM} electrodes have a lower PSS surface coverage than PEDOT:PSS_{ADD} electrodes. This reduction in the insulating PSS layer could result in a more efficient and homogeneous charge extraction by the PEDOT:PSS_{IMM} electrode. The increase in J_{sc} could also possibly be due to a change in the P3HT:PCBM blend segregation. It is well known that phase segregation occurs in polymer blends

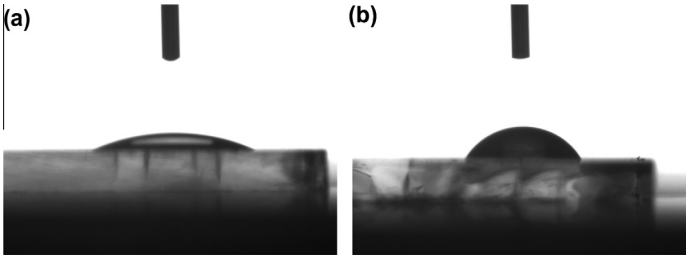

Fig. 4. Contact angle images for (a) PEDOT:PSS_{ADD} and (b) PEDOT:PSS_{IMM} electrodes.

Table 2
OPV device parameters for P3HT:PCBM OPV devices for ITO, PEDOT:PSS_{UT}, PEDOT:PSS_{ADD} and PEDOT:PSS_{IMM} electrodes. The standard deviation is shown in parentheses.

Electrode	J_{sc} (mA cm^{-2})	V_{oc} (V)	FF	PCE (%)
ITO	8.46 (0.59)	0.58 (0.01)	0.60 (0.03)	3.00 (0.21)
PEDOT:PSS_{UT}	0.63 (0.13)	0.58 (0.02)	0.27 (0.01)	0.10 (0.02)
PEDOT:PSS_{ADD}	6.62 (0.64)	0.59 (0.01)	0.63 (0.03)	2.42 (0.24)
PEDOT:PSS_{IMM}	7.15 (0.72)	0.59 (0.01)	0.64 (0.02)	2.66 (0.25)

and the lowest surface energy component (in this case P3HT) segregates to the free interface [40]. At the substrate/blend interface, however, the segregation is partly affected by the surface energy of the substrate. Substrates with a lower surface energy have been shown to favour lower surface energy components allowing minimisation of the free energy [41,42]. With PEDOT:PSS electrodes, we suggest that the lower surface energy of PEDOT:PSS_{IMM} electrodes promotes accumulation of P3HT towards the substrate/blend interface. This more favourable phase segregation for this regular P3HT:PCBM device architecture could result in a more efficient charge transport and collection enhancing the J_{sc}.

4. Conclusions

We have shown that the conductivity of PEDOT:PSS films can be further enhanced by treatment with the polar organic solvent DMSO. Two different DMSO treatments – addition and immersion – were explored in relation to the PEDOT and PSS composition on the electrode surface. Both PEDOT:PSS_{ADD} and PEDOT:PSS_{IMM} electrodes produced films with a similar R_{sheet}, but the treatments modified the PEDOT:PSS films in different ways. Immersing a PEDOT:PSS film in DMSO resulted in a large reduction in the amount of PSS seen on the electrode surface whereas adding DMSO to the PEDOT:PSS dispersion is thought to cause the PSS to rearrange within the film.

The effect of the different electrode treatments on P3HT:PCBM OPV device performance was also studied and compared to an ITO/PEDOT:PSS_{HTL} reference device. OPV devices fabricated on PEDOT:PSS_{IMM} electrodes outperformed those based on PEDOT:PSS_{ADD} electrodes. The larger PCE obtained on PEDOT:PSS_{IMM} electrodes was mainly due to an increase in J_{sc}. This study has indicated the potential for PEDOT:PSS electrodes as a possible low cost alternative electrode in OPV devices, while still obtaining a reasonable OPV device performance. Additionally, it highlights that while treatments may have a similar effect on the PEDOT:PSS conductivity, subtle differences in the electrode surface may make one treatment more compatible with a photoactive system than another.

Acknowledgements

This work was supported by the Engineering and Physical Sciences Research Council, UK (Grant Nos. EP/P50578X1 and EP/H021388/1) and Paintbox Limited. The Science City XPS system used in this research was funded through the Science City Advance Materials Project1: Creating and Characterising Next Generation of Advanced with support from AWM and ERDF funds.

Appendix A. Supplementary material

Supplementary data associated with this article can be found, in the online version, at http://dx.doi.org/10.1016/j.orgel.2014.07.015.

References

[1] M. Kaltenbrunner, M.S. White, E.D. Głowacki, T. Sekitani, T. Someya, N.S. Sariciftci, S. Bauer, Nat. Commun. 3 (2012) 770.
[2] J. You, L. Dou, K. Yoshimura, T. Kato, K. Ohya, T. Moriarty, K. Emery, C.-C. Chen, J. Gao, G. Li, Y. Yang, Nat. Commun. 4 (2013) 1446.
[3] M. Jørgensen, K. Norrman, S.A. Gevorgyan, T. Tromholt, B. Andreasen, F.C. Krebs, Adv. Mater. 24 (2012) 580–612.
[4] B. Azzopardi, C.J.M. Emmott, A. Urbina, F.C. Krebs, J. Mutale, J. Nelson, Energy Environ. Sci. 4 (2011) 3741–3753.
[5] J. Wu, H.A. Becerril, Z. Bao, Z. Liu, Y. Chen, P. Peumans, Appl. Phys. Lett. 92 (2008) 263302.
[6] M.W. Rowell, M.A. Topinka, M.D. McGehee, H.-J. Prall, G. Dennler, N.S. Sariciftci, L. Hu, G. Gruner, Appl. Phys. Lett. 88 (2006) 233506.
[7] H.M. Stec, R.A. Hatton, ACS Appl. Mater. Interfaces 4 (2012) 6013–6020.
[8] T. Aernouts, P. Vanlaeke, W. Geens, J. Poortmans, P. Heremans, S. Borghs, R. Mertens, R. Andriessen, L. Leenders, Thin Solid Films 451–452 (2004) 22–25.
[9] D.-S. Leem, A. Edwards, M. Faist, J. Nelson, D.D.C. Bradley, J.C. de Mello, Adv. Mater. 23 (2011) 4371–4375.
[10] S. Kirchmeyer, K. Reuter, J. Mater. Chem. 15 (2005) 2077–2088.
[11] US5300575 (Bayer AG).
[12] Y. Kim, A.M. Ballantyne, J. Nelson, D.D.C. Bradley, Org. Electron. 10 (2009) 205–209.
[13] S. Khodabakhsh, B.M. Sanderson, J. Nelson, T.S. Jones, Adv. Funct. Mater. 16 (2006) 95–100.
[14] M.P.d. Jong, L.J.v. IJzendoorn, M.J.A.d. Voigt, Appl. Phys. Lett. 77 (2000) 2255–2257.
[15] E. Voroshazi, B. Verreet, A. Buri, R. Müller, D. Di Nuzzo, P. Heremans, Org. Electron. 12 (2011) 736–744.
[16] M. Vosgueritchian, D.J. Lipomi, Z. Bao, Adv. Funct. Mater. 22 (2012) 421–428.
[17] C. Badre, L. Marquant, A.M. Alsayed, L.A. Hough, Adv. Funct. Mater. 22 (2012) 2723–2727.
[18] A.M. Nardes, M. Kemerink, M.M. de Kok, E. Vinken, K. Maturova, R.A.J. Janssen, Org. Electron. 9 (2008) 727–734.
[19] J.Y. Kim, J.H. Jung, D.E. Lee, J. Joo, Synth. Met. 126 (2002) 311–316.
[20] Y. Xia, K. Sun, J. Ouyang, Adv. Mater. 24 (2012) 2436–2440.
[21] Y. Xia, J. Ouyang, J. Mater. Chem. 21 (2011) 4927–4936.
[22] D. Alemu, H.-Y. Wei, K.-C. Ho, C.-W. Chu, Energy Environ. Sci. (2012).
[23] Y.H. Kim, C. Sachse, M.L. Machala, C. May, L. Müller-Meskamp, K. Leo, Adv. Funct. Mater. 21 (2011) 1076–1081.
[24] I. Cruz-Cruz, M. Reyes-Reyes, M.A. Aguilar-Frutis, A.G. Rodriguez, R. López-Sandoval, Synth. Met. 160 (2010) 1501–1506.
[25] X. Crispin, S. Marciniak, W. Osikowicz, G. Zotti, A.W.D. van der Gon, F. Louwet, M. Fahlman, L. Groenendaal, F. De Schryver, W.R. Salaneck, J. Polym. Sci., Part B: Polym. Phys. 41 (2003) 2561–2583.
[26] S.-I. Na, G. Wang, S.-S. Kim, T.-W. Kim, S.-H. Oh, B.-K. Yu, T. Lee, D.-Y. Kim, J. Mater. Chem. 19 (2009) 9045–9053.

[27] J. Ouyang, Q. Xu, C.-W. Chu, Y. Yang, G. Li, J. Shinar, Polymer 45 (2004) 8443–8450.
[28] N. Kim, B.H. Lee, D. Choi, G. Kim, H. Kim, J.-R. Kim, J. Lee, Y.H. Kahng, K. Lee, Phys. Rev. Lett. 109 (2012) 106405.
[29] G. Greczynski, T. Kugler, M. Keil, W. Osikowicz, M. Fahlman, W.R. Salaneck, J. Electron Spectrosc. Relat. Phenom. 121 (2001) 1–17.
[30] Y.H. Kim, C. Sachse, M. Hermenau, K. Fehse, M. Riede, L. Muller-Meskamp, K. Leo, Appl. Phys. Lett. 99 (2011) 113305.
[31] L.A.A. Pettersson, S. Ghosh, O. Inganäs, Org. Electron. 3 (2002) 143–148.
[32] G. Greczynski, T. Kugler, W.R. Salaneck, Thin Solid Films 354 (1999) 129–135.
[33] T.-W. Lee, Y. Chung, Adv. Funct. Mater. 18 (2008) 2246–2252.
[34] L.S.C. Pingree, B.A. MacLeod, D.S. Ginger, J. Phys. Chem. C 112 (2008) 7922–7927.
[35] X.-D. Dang, M. Dante, T.-Q. Nguyen, Appl. Phys. Lett. 93 (2008) 241911.
[36] N.K. Unsworth, I. Hancox, C. Argent Dearden, T. Howells, P. Sullivan, R.S. Lilley, J. Sharp, T.S. Jones, Appl. Phys. Lett. 103 (2013).
[37] J. Ouyang, C.W. Chu, F.C. Chen, Q. Xu, Y. Yang, Adv. Funct. Mater. 15 (2005) 203–208.
[38] X. Crispin, F.L.E. Jakobsson, A. Crispin, P.C.M. Grim, P. Andersson, A. Volodin, C. van Haesendonck, M. Van der Auweraer, W.R. Salaneck, M. Berggren, Chem. Mater. 18 (2006) 4354–4360.
[39] D.S. Germack, C.K. Chan, B.H. Hamadani, L.J. Richter, D.A. Fischer, D.J. Gundlach, D.M. DeLongchamp, Appl. Phys. Lett. 94 (2009).
[40] C.M. Björström, S. Nilsson, A. Bernasik, A. Budkowski, M. Andersson, K.O. Magnusson, E. Moons, Appl. Surf. Sci. 253 (2007) 3906–3912.
[41] D.H.K. Pan, W.M. Prest, J. Appl. Phys. 58 (1985) 2861–2870.
[42] X. Wang, T. Ederth, O. Inganäs, Langmuir 22 (2006) 9287–9294.